

NODAL AUXILIARY SPACE PRECONDITIONERS FOR MIXED VIRTUAL ELEMENT METHODS *

WIETSE M. BOON¹ AND ERIK NILSSON²

Abstract. We propose nodal auxiliary space preconditioners for facet and edge virtual elements of lowest order by deriving discrete regular decompositions on polytopal grids and generalizing the Hiptmair-Xu preconditioner to the virtual element framework. The preconditioner consists of solving a sequence of elliptic problems on the nodal virtual element space, combined with appropriate smoother steps. Under assumed regularity of the mesh, the preconditioned system is proven to have bounded spectral condition number independent of the mesh size and this is verified by numerical experiments on a sequence of polygonal meshes. Moreover, we observe numerically that the preconditioner is robust on meshes containing elements with high aspect ratios.

2010 Mathematics Subject Classification. 65N30, 65N85, 65N22.

The dates will be set by the publisher.

1. INTRODUCTION

The Virtual Element Method (VEM) is a discretization method that handles polytopal grids without requiring explicit knowledge of the local basis functions. The method was initially introduced as a generalization of the Finite Element Method, leading to discrete spaces that are proper subspaces of the Sobolev space H^1 [4, 5]. Subsequently, well-known *mixed* finite elements were generalized to the VEM framework and discrete subspaces of H^{div} and H^{curl} have been proposed, with applications in porous media flow and electromagnetism [9, 16–18].

Similar to (mixed) finite element methods, the condition number of the linear system obtained from VEM depends on the quality of the mesh, in particular on the mesh size and the aspect ratios of its elements. This poses a problem for iterative solvers in case the problem is too large for direct solvers to handle. The performance of these solvers is directly affected by the ill conditioning of the system matrix and smaller mesh sizes may lead to larger numbers of iterations before convergence. The main objective of this work is to construct preconditioners for systems discretized by mixed virtual element methods that are robust with respect to the mesh size.

We follow the framework of auxiliary space preconditioning [28], and in particular formulate a generalization of the Hiptmair-Xu preconditioner [22] for mixed virtual element methods of lowest order. The main advantage of this approach is that the original problem, posed on facet or edge spaces, is replaced by a series of elliptic problems posed on the nodal virtual space. The nodal space is the most well understood virtual element space and several efficient iterative solvers for such problems are available in the literature [2, 6, 11].

Keywords and phrases: auxiliary space preconditioning, Hiptmair-Xu preconditioner, mixed virtual element methods

* WMB was supported by the European Union's Horizon 2020 research and innovation programme under the Marie Skłodowska-Curie grant agreement No. 101031434 – MiDiROM. EN was supported by Swedish Research Council Grant No. 2018-05262 and the Wallenberg Academy Fellowship KAW 2019.0190.

¹ NORCE Norwegian Research Centre, N-5838 Bergen, Norway, E-mail: wibo@norceresearch.no

² Department of Mathematics, KTH Royal Institute of Technology, SE-100 44 Stockholm, Sweden. E-mail: erikni6@kth.se

It is important to note that the theoretical results presented herein only cover regular meshes containing convex elements with mild aspect ratios. However, the Hiptmair-Xu preconditioner in the case of finite elements often performs robustly in the presence of badly shaped elements as well [10]. If this behavior is inherited to the virtual element case, then the proposed preconditioner will enable us to handle a wider class of polyhedral grids. In this context, we are interested in grids that are adapted from a background mesh to conform to interfaces or features that are arbitrarily placed in the computational domain. Such grid adaptations often result in arbitrarily shaped polygons and a robust preconditioner may be key in handling the corresponding, ill-conditioned systems. We investigate these possibilities numerically in Section 5.

We note that the virtual element method can handle elements with high aspect ratios by augmenting the stabilization term, see e.g. [25] for an overview on this strategy. In contrast, our preconditioning approach leaves the discretization method intact and is therefore less intrusive. We furthermore mention that parallel solvers for mixed virtual element methods were previously proposed in [19]. In comparison to that work, our proposed preconditioners have a strong theoretical foundation, which allows us to rigorously prove robustness with respect to the mesh size. Finally, auxiliary space preconditioners for linear, nodal VEM were introduced in [29]. The difference with that work is that we propose a construction based on a regular decomposition, instead of a simplicial subtesselation of the mesh.

The main contributions of this work are summarized as follows:

- We derive stable, regular decompositions of the facet and edge virtual element spaces of lowest order.
- We propose a Hiptmair-Xu preconditioner for elliptic problems that consists of continuous transfer operators, continuous smoothers, and a sequence of elliptic problems on the nodal virtual element space. The condition number of the preconditioned system is proven to be independent of the mesh size.
- Numerical experiments in 2D validate the theoretical results and moreover indicate robust performance in the presence of elements with high aspect ratios.

Moreover, the following observations serve as additional contributions. First, we use the regular decomposition to provide an alternative proof that the lowest order conforming VE spaces form an exact co-chain complex in Theorem 3.4. Second, we observe in Section 4.2.1 that the stabilization term that is common to virtual element methods has the sufficient properties to serve as a suitable smoother. Third, we used the smoothers to derive inverse inequalities for the lowest order facet and edge virtual element spaces in Corollary 4.3.

This article is organized as follows. First, Section 2 introduces the relevant concepts from Sobolev theory, differential complexes, and VEM. In Section 3, we place the lowest order VE spaces in the context of co-chain complexes and prove the discrete regular decomposition. The framework of auxiliary space preconditioning is introduced in Section 4 with which we construct the preconditioner and prove its robustness. Section 5 contains the numerical experiments that validate the theory and showcase the performance of the preconditioner. Conclusions are presented in Section 6.

2. PRELIMINARIES AND NOTATION

In this section, we introduce the notation conventions and present several key results from functional analysis and VE theory. The definitions concerning the relevant function spaces are summarized at the end of the section in Table 2.1, for convenience.

2.1. Continuous function spaces

Let $\Omega \subset \mathbb{R}^n$ with $n \in \{2, 3\}$ be a bounded, contractible domain with Lipschitz boundary $\partial\Omega$. Let \vec{n} denote the outward oriented unit vector that is normal to $\partial\Omega$. $L^2(\Omega)$ denotes the Hilbert space consisting of square-integrable functions on Ω , endowed with inner product (\cdot, \cdot) and norm $\|\cdot\|$. With a slight abuse of notation, we reuse (\cdot, \cdot) and $\|\cdot\|$ for analogous

inner product and norm on vector-valued distributions. We moreover define:

$$H^1(\Omega) := \{v \in L^2(\Omega) : \text{grad } v \in [L^2(\Omega)]^n\}, \quad H^{\text{div}}(\Omega) := \{v \in [L^2(\Omega)]^n : \text{div } v \in L^2(\Omega)\}, \quad (2.1a)$$

$$H^{\text{curl}}(\Omega) := \begin{cases} \{v \in [L^2(\Omega)]^3 : \text{curl } v \in [L^2(\Omega)]^3\}, & n = 3, \\ H^1(\Omega), & n = 2. \end{cases} \quad (2.1b)$$

The subspaces relevant for problems with essential boundary conditions are defined as follows:

$$H_0^1(\Omega) := \{v \in H^1(\Omega) : v|_{\partial\Omega} = 0\}, \quad H_0^{\text{div}}(\Omega) := \{v \in H^{\text{div}}(\Omega) : v \cdot \bar{n}|_{\partial\Omega} = 0\}, \quad (2.2a)$$

$$H_0^{\text{curl}}(\Omega) := \begin{cases} \{v \in H^{\text{curl}}(\Omega) : \bar{n} \times v|_{\partial\Omega} = 0\}, & n = 3, \\ H_0^1(\Omega), & n = 2. \end{cases} \quad L^2(\Omega)/\mathbb{R} := \left\{v \in L^2(\Omega) : \int_{\Omega} v = 0\right\}. \quad (2.2b)$$

Remark 2.1 (The two-dimensional curl). *While we aim to employ a unified treatment with respect to dimension, the definition of the curl in 2D requires some additional details. For a scalar field p and a vector field $v = (v_1, v_2)$ we define, respectively,*

$$\text{curl } p := \text{grad}^{\perp} p = (-\partial_2 p, \partial_1 p), \quad \text{curl } v := \text{div } v^{\perp} = \partial_2 v_1 - \partial_1 v_2, \quad (2.3a)$$

in which the superscript \perp denotes a counter clockwise rotation of a vector by $\pi/2$.

2.2. Model problems

The problems of interest are the projection problems onto the Sobolev spaces introduced in Section 2.1. Namely, given $f \in [L^2(\Omega)]^n$,

$$\text{Find } u \in H^{\text{div}}(\Omega) : \quad (u, v) + (\text{div } u, \text{div } v) = (f, v), \quad \forall v \in H^{\text{div}}(\Omega), \quad (2.4)$$

$$\text{Find } u \in H^{\text{curl}}(\Omega) : \quad (u, v) + (\text{curl } u, \text{curl } v) = (f, v), \quad \forall v \in H^{\text{curl}}(\Omega). \quad (2.5)$$

For the numerical validation of the preconditioner, we will in addition to (2.4) consider the mixed formulation of the Poisson problem, also known as the Darcy problem. In weak form it reads as follows: given $f \in L^2(\Omega)^n$ and $g \in L^2(\Omega)$, find $u \in H^{\text{div}}(\Omega)$ and $p \in L^2(\Omega)$ such that

$$(u, v) - (p, \text{div } v) = (f, v), \quad \forall v \in H^{\text{div}}(\Omega), \quad (2.6a)$$

$$-(q, \text{div } u) = (g, q), \quad \forall q \in L^2(\Omega). \quad (2.6b)$$

2.3. Exact co-chain complexes

A co-chain complex $(V^{\bullet}, d^{\bullet})$ is a sequence of linear spaces V^k and differential maps $d^k : V^k \rightarrow V^{k+1}$ with the property $d^{k+1}d^k = 0$ for all k . We will omit the superscript on d for national brevity when k is clear from context. A co-chain complex can be illustrated as the following sequence, in which two consecutive steps in the diagram map to zero:

$$\dots \rightarrow V^{k-1} \xrightarrow{d} V^k \xrightarrow{d} V^{k+1} \rightarrow \dots \quad (2.7)$$

We will focus on complexes that only have non-trivial V^k for $0 \leq k \leq n$ with n the dimension of the domain Ω . For $n = 3$, we thus consider a specific instance of (2.7) given by:

$$0 \rightarrow V^{n-3} \xrightarrow{d} V^{n-2} \xrightarrow{d} V^{n-1} \xrightarrow{d} V^n \rightarrow 0. \quad (2.8)$$

In the following, we will thus have $V^k = 0$ and $d^k = 0$ for all $k \notin [0, n]$.

Since $dd = 0$ by definition, we have $dV^k \subseteq \ker_d V^{k+1}$ in which $\ker_d V^{k+1}$ denotes the null space $\{v \in V^{k+1} : dv = 0\}$. We refer to the co-chain complex as *exact* if the converse inclusion holds as well, i.e. if

$$dV^k = \ker_d V^{k+1}, \quad (2.9)$$

In this work, we focus on spaces V^k that are subsets of $L^2(\Omega)$ and we therefore endow each V^k with the following graph norm:

$$\|v\|_{V^k}^2 := \|v\|^2 + \|dv\|^2. \quad (2.10)$$

The following important result follows directly from the exactness of a co-chain complex.

Lemma 2.1 (Poincaré inequality [3, Thm. 4.6]). *If a co-chain complex (V^\bullet, d) is exact, then:*

$$\|v\| \lesssim \|dv\|, \quad \forall v \perp \ker_d V^k. \quad (2.11)$$

A consequence of Lemma 2.1 is the following result.

Lemma 2.2 (Stable potentials). *Let (V^\bullet, d) be an exact co-chain complex. Then, for $v \in V^k$ with $dv = 0$, there exists a potential $u \in V^{k-1}$ that satisfies*

$$du = v, \quad \|u\|_{V^{k-1}} \lesssim \|v\|. \quad (2.12)$$

Proof. First, by exactness, there exists a $\bar{u} \in V^{k-1}$ for which $d\bar{u} = v$. Next, we note that the space V^{k-1} can be decomposed as

$$V^{k-1} = \ker_d(V^{k-1}) \oplus \ker_d(V^{k-1})^\perp \quad (2.13)$$

and thus we may write $\bar{u} = z + u$ with $z \in \ker_d(V^{k-1})$ and $u \perp \ker_d(V^{k-1})$. In turn, it follows that

$$du = d(\bar{u} - z) = d\bar{u} = v. \quad (2.14)$$

Using once more that the complex is exact, we invoke Lemma 2.1 on $u \perp \ker_d(V^{k-1})$ to obtain the result. (Since $du = v$, it is clear that we also have $\|du\| \lesssim \|v\|$.) \square

We focus on a specific co-chain complex, known as the de Rham complex on Ω . The two- and three-dimensional cases are as follows:

$$0 \hookrightarrow H^1(\Omega)/\mathbb{R} \xrightarrow{\text{grad}} H^{\text{curl}}(\Omega) \xrightarrow{\text{curl}} H^{\text{div}}(\Omega) \xrightarrow{\text{div}} L^2(\Omega) \rightarrow 0, \quad n = 3, \quad (2.15a)$$

$$0 \hookrightarrow H^1(\Omega)/\mathbb{R} \xrightarrow{\text{curl}} H^{\text{div}}(\Omega) \xrightarrow{\text{div}} L^2(\Omega) \rightarrow 0, \quad n = 2. \quad (2.15b)$$

These complexes are appropriate for handling natural boundary conditions on $\partial\Omega$. If essential boundary conditions are needed, we use the spaces H_0^\bullet from (2.2) and consider the complexes:

$$0 \hookrightarrow H_0^1(\Omega) \xrightarrow{\text{grad}} H_0^{\text{curl}}(\Omega) \xrightarrow{\text{curl}} H_0^{\text{div}}(\Omega) \xrightarrow{\text{div}} L^2(\Omega)/\mathbb{R} \rightarrow 0, \quad n = 3, \quad (2.16a)$$

$$0 \hookrightarrow H_0^1(\Omega) \xrightarrow{\text{curl}} H_0^{\text{div}}(\Omega) \xrightarrow{\text{div}} L^2(\Omega)/\mathbb{R} \rightarrow 0, \quad n = 2. \quad (2.16b)$$

From now on, we define V^k and d such that (2.8) corresponds to one of these four complexes, each of which is exact since Ω is contractible [3]. More precisely, we define V^n as the rightmost L^2 space and V^{n-1} will be the H^{div} to its left. The notation V^{n-2} will only be used for $n = 3$. Finally, V^0 will refer to the H^1 space in the left of the complex.

A summary of V^k and all other function spaces introduced in this section is provided in Table 2.1 at the end of the section.

We emphasize that the graph norm $\|\cdot\|_{V^k}$ from (2.10) coincides with the norms conventionally assigned to the corresponding Sobolev spaces. For example, we have $\|v\|_{V^{n-1}}^2 = \|v\|^2 + \|\operatorname{div} v\|^2 =: \|v\|_{H^{\operatorname{div}}}^2$ and $\|p\|_{V^n} = \|p\|$. Moreover, the projection problems from Section 2.2 can be rewritten as: Given f , find $u \in V^k$ such that

$$(u, v) + (du, dv) = (f, v), \quad \forall v \in V^k. \quad (2.17)$$

2.4. Regular decomposition

A key tool in the construction of nodal auxiliary space preconditioners is the existence of a decomposition into functions of higher regularity. For that, we introduce the following subspace $W^k \subseteq V^k$ for each k :

$$W^k := [H^1(\Omega)]^{\binom{n}{k}} \cap V^k. \quad (2.18)$$

We emphasize that $W^n, W^0 \subseteq H^1(\Omega)$ while $W^k \subseteq [H^1(\Omega)]^n$ for $0 < k < n$, if $n = 2, 3$. The intersection with V^k ensures that the functions in W^k satisfy the boundary conditions in the case of complex (2.16). The regular decomposition of V^k is presented in the following lemma.

Lemma 2.3 (Continuous regular decomposition [22, Lem. 3.10]). *Given $v \in V^k$, then $\psi \in W^k$ and $p \in V^{k-1}$ exist such that*

$$v = \psi + dp, \quad \|\psi\|_1 \lesssim \|dv\|, \quad \|p\|_{V^{k-1}} \lesssim \|v\|_{V^k}. \quad (2.19)$$

2.5. Virtual element spaces of lowest order

We will now introduce the necessary discrete concepts. Let \mathcal{T}_h be a polytopal tessellation of Ω . For the geometry we use the following nomenclature. An element K is n -dimensional, a facet is $(n-1)$ -dimensional, an edge is of dimension 1, and a node is 0-dimensional. For K an element of \mathcal{T}_h , let $\mathcal{F}(K)$ be the set of facets that compose ∂K , $\mathcal{E}(K)$ the set of the corresponding edges, and $\mathcal{N}(K)$ the set of nodes neighboring K . The sets of all facets, edges, and nodes of \mathcal{T}_h are then defined as:

$$\mathcal{F} := \bigcup_{K \in \mathcal{T}_h} \mathcal{F}(K), \quad \mathcal{E} := \bigcup_{K \in \mathcal{T}_h} \mathcal{E}(K), \quad \mathcal{N} := \bigcup_{K \in \mathcal{T}_h} \mathcal{N}(K). \quad (2.20)$$

To each facet $F \in \mathcal{F}$ we associate a unique normal vector \vec{n} and to each edge $E \in \mathcal{E}$ a unit tangential vector \vec{t} .

Assumption 2.1. *The polytopal mesh \mathcal{T}_h satisfies the following two conditions:*

- (1) *There exists a constant $h > 0$ such that each mesh entity σ of dimension $n_\sigma \geq 1$ has diameter $\operatorname{diam}(\sigma) \approx h$ and measure $|\sigma| \approx h^{n_\sigma}$.*
- (2) *Every element $K \in \mathcal{T}_h$ and every facet $F \in \mathcal{F}(K)$ is a strictly convex polytope.*

The relation $a \lesssim b$ implies that a constant $C > 0$ exists, independent of the mesh size h , such that $Ca \leq b$. The converse $a \gtrsim b$ is defined similarly and we denote $a \approx b$ if $a \lesssim b \lesssim a$.

Let us continue by considering the local virtual element spaces $V_h^k(K)$ with $0 \leq k \leq n$ and $K \in \mathcal{T}_h$ an element. We start by defining $V_h^n(K)$ as the space of constants, with dof_K^n the associated degree of freedom:

$$V_h^n(K) := \mathbb{P}_0(K), \quad \operatorname{dof}_K^n(v) := \int_K v. \quad (2.21)$$

The next local VE spaces on K (cf. [14, 15, 18]) are of finite dimension, but contain functions that are not necessarily polynomials. Let the facet VE space $V_h^{n-1}(K)$ that generalizes the Raviart-Thomas element [27] be given by

$$\begin{aligned} V_h^{n-1}(K) &:= \{v \in [L^2(K)]^2 : \operatorname{div} v \in \mathbb{P}_0(K), \operatorname{curl} v \in \mathbb{P}_0(K), \\ &\quad (v \cdot \vec{n})|_F \in \mathbb{P}_0(F) \forall F \in \mathcal{F}(K), \int_K v \cdot \vec{x}_K^\perp = 0\}, \quad n = 2, \end{aligned} \quad (2.22a)$$

$$\begin{aligned} V_h^{n-1}(K) &:= \{v \in [L^2(K)]^3 : \operatorname{div} v \in \mathbb{P}_0(K), \operatorname{curl} v \in [\mathbb{P}_0(K)]^3, \\ &\quad (v \cdot \vec{n})|_F \in \mathbb{P}_0(F) \forall F \in \mathcal{F}(K), \int_K v \cdot (\vec{x}_K \times \vec{y}) = 0 \forall \vec{y} \in [\mathbb{P}_0(K)]^3\}, \quad n = 3, \end{aligned} \quad (2.22b)$$

in which $\vec{x}_K := \vec{x} - \vec{c}_K$ with \vec{c}_K the centroid of K . This space has one degree of freedom on each facet, given by

$$\operatorname{dof}_F^{n-1}(v) := \int_F v \cdot \vec{n}, \quad \forall F \in \mathcal{F}. \quad (2.22c)$$

Next, we introduce the edge VE space for $n = 3$, which is similar to the Nédélec edge element of the first kind [26]:

$$\begin{aligned} V_h^{n-2}(K) &:= \{v \in [L^2(K)]^3 : \operatorname{div} v = 0, \operatorname{curl} \operatorname{curl} v \in [\mathbb{P}_0(K)]^3, \\ &\quad (\vec{n} \times v)|_F \in V_h^{n-2}(F) \forall F \in \mathcal{F}(K), \\ &\quad (v|_F \cdot \vec{t})|_E = (v|_{F'} \cdot \vec{t})|_E \forall E \in \mathcal{E}(F) \cap \mathcal{E}(F') \text{ with } F, F' \in \mathcal{F}(K), \\ &\quad \int_K \operatorname{curl} v \cdot (\vec{x}_K \times \vec{y}) = 0 \forall \vec{y} \in [\mathbb{P}_0(K)]^3\} \end{aligned} \quad (2.23a)$$

In this case, the degrees of freedom are defined on the edges of the mesh:

$$\operatorname{dof}_E^{n-2}(v) := \int_E v \cdot \vec{t}, \quad \forall E \in \mathcal{E}(K). \quad (2.23b)$$

Lastly, we the VE nodal space, which generalizes the Lagrange finite element, is given by

$$V_h^0(K) := \{v \in C^0(K) : \Delta v \in \mathbb{P}_0(K), v|_F \in \mathbb{P}_1(F) \forall F \in \mathcal{F}(K), \int_K \operatorname{grad} v \cdot \vec{x}_K = 0\}, \quad n = 2, \quad (2.24a)$$

$$V_h^0(K) := \{v \in C^0(K) : \Delta v = 0, v|_F \in V_h^0(F) \forall F \in \mathcal{F}(K)\}, \quad n = 3, \quad (2.24b)$$

endowed with the degrees of freedom:

$$\operatorname{dof}_{\vec{x}}^0(v) := v(\vec{x}), \quad \forall \vec{x} \in \mathcal{N}(K). \quad (2.24c)$$

Let us remark on a convenient property that all $V_h^k(K)$ share, namely that they are each locally H^1 -regular.

Lemma 2.4 (Local H^1 -regularity). *For each $K \in \mathcal{T}_h$, it holds that $V_h^k(K) \subset W^k(K)$.*

Proof. We first show that $\Delta v \in \mathbb{P}_0(K)$ for all $v \in V_h^k(K)$. We distinguish the four cases:

- ($k = n$) The definition $v \in V_h^n(K) := \mathbb{P}_0(K)$ directly gives us $\Delta v = 0$.
- ($k = n - 1$) Recall the following calculus identity, which holds for $n = 2, 3$:

$$\Delta v = -\operatorname{curl}(\operatorname{curl} v) + \operatorname{grad}(\operatorname{div} v). \quad (2.25)$$

From (2.22), we immediately obtain $\Delta v = 0$.

- ($k = n - 2, n = 3$) Using (2.25), the properties (2.23) gives us $\Delta v \in \mathbb{P}_0(K)$.
- ($k = 0$) The definitions (2.24) imply $\Delta v \in \mathbb{P}_0(K)$ for both $n = 2, 3$.

We now conclude that v is the solution to a Poisson problem with boundary data given by the degrees of freedom, which provides the result. \square

Finally, the global VE spaces are defined on the mesh \mathcal{T}_h as

$$V_h^k := \{w_h \in V^k : w_h|_K \in V_h^k(K), \forall K \in \mathcal{T}_h\}. \quad (2.26)$$

Note that, by construction, the discrete spaces are conforming, i.e. $V_h^k \subseteq V^k$ for all k .

2.5.1. Useful inequalities for virtual element spaces

For ease of reference, we mention several inequalities that were derived for the VE spaces.

Lemma 2.5 (Nodal inverse inequalities [13, Thm. 3.6], [23]). *Let $n = 2, 3$ and consider $K \in \mathcal{T}_h$. For each $w \in V_h^0(K)$, it holds that*

$$|w|_{1,K} \lesssim h^{-1} \|w\|_K. \quad (2.27a)$$

We also have the nodal VEM trace inequalities which follow from the inverse inequalities.

Lemma 2.6 (Nodal trace inequalities). *Let $w \in V_h^0(K)$. It holds that*

$$\|w\|_E \lesssim h^{-1/2} \|w\|_F, \quad F \in \mathcal{F}, E \in \mathcal{E}, \quad n = 3, \quad (2.28a)$$

$$\|w\|_F \lesssim h^{-1/2} \|w\|_K, \quad K \in \mathcal{T}_h, F \in \mathcal{F}, \quad n = 2, 3. \quad (2.28b)$$

Proof. Note that $w|_F \in V_h^0(F)$. For each case we get then the result in two steps:

$$\|w\|_E \lesssim h^{1/2} |w|_{1,F} + h^{-1/2} \|w\|_F \lesssim h^{-1/2} \|w\|_F, \quad F \in \mathcal{F}, E \in \mathcal{E}, \quad (2.29a)$$

$$\|w\|_F \lesssim h^{1/2} |w|_{1,K} + h^{-1/2} \|w\|_K \lesssim h^{-1/2} \|w\|_K, \quad K \in \mathcal{T}_h, F \in \mathcal{F}. \quad (2.29b)$$

The first inequality is the continuous scaled trace inequality valid for functions in $H^1(F)$ respectively $H^1(K)$, see [8, (2.4)] and [14, Lemma 2.1]. The second is due to Lemma 2.5. \square

We recall some more useful results.

Lemma 2.7 (VEM stabilization operators [14, Prop. 5.2, Thm. A.2, Prop. 5.5]). *For $K \in \mathcal{T}_h$ it holds that*

$$\|v_h\|_K^2 \approx h \sum_{F \in \mathcal{F}(K)} (v_h \cdot \vec{n}, v_h \cdot \vec{n})_F, \quad v \in V_h^{n-1}, \quad (2.30)$$

$$\|v_h\|_K^2 \approx h^2 \sum_{E \in \mathcal{E}(K)} (v_h \cdot \vec{t}, v_h \cdot \vec{t})_E, \quad v \in V_h^{n-2}, n = 3. \quad (2.31)$$

2.5.2. The auxiliary nodal space

Recall the subspace W^k containing H^1 -regular functions from (2.18). To facilitate a discrete version of the regular decomposition from Lemma 2.3, we introduce a nodal space that captures H^1 -regular (vector) functions:

$$W_h^k := \left\{ w_h \in W^k : w_h|_K \in [V_h^0(K)]^{\binom{n}{k}}, \forall K \in \mathcal{T}_h \right\}. \quad (2.32)$$

Note that this space contains vector-valued functions for $0 < k < n$, and otherwise scalar-valued functions. We emphasize that these spaces have global H^1 -regularity; $W_h^k \subset W^k$ for all k . Moreover, the inverse (Lemma 2.5) and trace (Lemma 2.6) estimates hold for $0 < k < n$ by applying them component-wise.

2.5.3. A space of regular potentials

We conclude this section with another convenient subspace of W^k , consisting of H^1 -regular potentials of discrete functions:

$$X^k := \left\{ w \in W^k : dw \in V_h^{k+1} \right\}. \quad (2.33)$$

Remark 2.2. We note that X^k is nontrivial and we will construct specific elements of X^k in Theorems 3.4 and 3.11.

For ease of reference, we summarize the function spaces introduced in this section in Table 2.1.

TABLE 2.1. Instances of the spaces V_h^k , W_h^k , and X^k , for the complex with natural boundary conditions (2.15) and $n = 3$.

k	V^k	V_h^k	W_h^k	X^k
0	H^1/\mathbb{R}	Nodal space	Nodal space	Potentials $v \in H^1$ with $\text{grad } v \in V_h^{n-2}$
$n-2$	H^{curl}	Edge space	Vector nodal space	Potentials $v \in [H^1]^3$ with $\text{curl } v \in V_h^{n-1}$
$n-1$	H^{div}	Face space	Vector nodal space	Potentials $v \in [H^1]^3$ with $\text{div } v \in V_h^n$
n	L^2	Piecewise constants	Nodal space	Potentials $v \in H^1$

3. REGULAR DECOMPOSITION FOR VIRTUAL ELEMENTS

In this section we develop the notions of co-chain complex and regular decomposition in the discrete setting, which are essential for our construction of nodal auxiliary space preconditioners. We show that the virtual element method forms a discrete co-chain complex, and that the canonical interpolation operators are stable co-chain projections. With the help of a Clément interpolant, we then derive the stable discrete regular decomposition.

3.1. A discrete co-chain complex

We continue by placing the discrete virtual element spaces from Section 2.5, illustrated in Figure 1, in the context of co-chain complexes from Section 2.3. Several results presented in this section have been shown for three-dimensional virtual element spaces in [15, 18]. While the two-dimensional analogues can be derived as boundary cases, we include the proofs here for completeness.

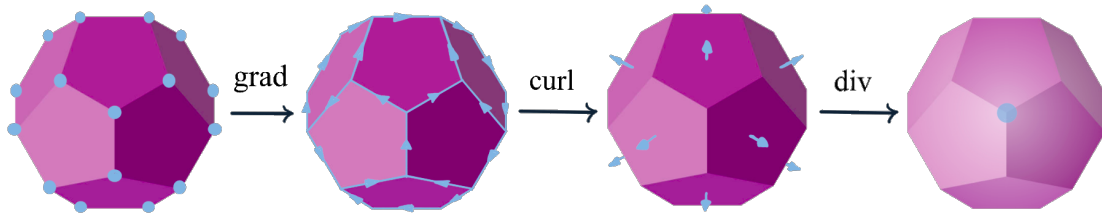


FIGURE 1. A discrete co-chain complex formed by the nodal, edge, facet, and cell virtual element spaces V_h^k on a regular dodecahedron.

Lemma 3.1. For V_h^k defined in Section 2.5, let d be the differential corresponding to Sobolev space V^k from Section 2.3. Then (V_h^*, d) is a co-chain complex:

$$dV_h^k \subseteq \ker_d(V_h^{k+1}). \quad (3.1)$$

Proof. The result was shown for $n = 3$ in [15, 18], so we continue with $n = 2$. Since $dd = 0$, it suffices to show that $dV_h^k \subseteq V_h^{k+1}$. Let us consider the two non-trivial cases for an element $K \in \mathcal{T}_h$:

- ($k = 0$) Let $v \in V_h^0(K)$ and $w := \text{curl } v$. We confirm that $w \in V_h^{n-1}(K)$ according to definition (2.23). First, we immediately have $\text{div } w = 0$. Second, $\text{curl } w = \Delta v \in \mathbb{P}_0(K)$ by (2.24). Third, on a facet F , we have $w \cdot \vec{n} = \nabla v \cdot \vec{t} \in \mathbb{P}_0(F)$ since $v|_F \in \mathbb{P}_1(F)$ by definition of $V_h^0(K)$. Lastly

$$\int_K w \cdot \vec{x}_K^\perp = \int_K \text{grad } v \cdot \vec{x}_K = 0. \quad (3.2)$$

- ($k = 1$) Let $v \in V_h^{n-1}(K)$, then $\text{div } v \in \mathbb{P}_0(K) = V_h^n(K)$ by (2.22).

Hence $dV_h^k(K) \subseteq V_h^{k+1}(K)$ locally on each $K \in \mathcal{T}_h$. Moreover, $dd = 0$ implies that $dV_h^k \subseteq V_h^{k+1}$ globally and the result follows by the definition (2.26). \square

3.2. Stable co-chain projections

Each V_h^k is endowed with a canonical interpolation operator $\Pi_h^k : [C^\infty(\Omega)]^{\binom{n}{k}} \rightarrow V_h^k$, which is defined as follows using the degrees of freedom dof_j^k and basis functions b_j :

$$[C^\infty(\Omega)]^{\binom{n}{k}} \ni v \mapsto \sum_{j=1}^{\dim V_h^k} \text{dof}_j^k(v) b_j \in V_h^k. \quad (3.3)$$

Note that each Π_h^k corresponds to an L^2 -projection onto a k -dimensional mesh entity. We refer to an operator Π_h^k as a *co-chain projection* if it commutes with the differential operator [3]. This commuting property is visualized by the following diagram:

$$\begin{array}{ccccccc} 0 & \hookrightarrow & C^\infty(\Omega)/\mathbb{R} & \xrightarrow{\text{grad}} & C^\infty(\Omega)^3 & \xrightarrow{\text{curl}} & C^\infty(\Omega)^3 & \xrightarrow{\text{div}} & C^\infty(\Omega) & \longrightarrow & 0 \\ & & \downarrow \Pi_h^0 & & \downarrow \Pi_h^{n-2} & & \downarrow \Pi_h^{n-1} & & \downarrow \Pi_h^n & & \\ 0 & \hookrightarrow & V_h^0 & \xrightarrow{\text{grad}} & V_h^{n-2} & \xrightarrow{\text{curl}} & V_h^{n-1} & \xrightarrow{\text{div}} & V_h^0 & \longrightarrow & 0 \end{array} \quad n=3 \quad (3.4a)$$

$$\begin{array}{ccccccc} 0 & \hookrightarrow & C^\infty(\Omega)/\mathbb{R} & \xrightarrow{\text{curl}} & C^\infty(\Omega)^2 & \xrightarrow{\text{div}} & C^\infty(\Omega) & \longrightarrow & 0 \\ & & \downarrow \Pi_h^0 & & \downarrow \Pi_h^{n-1} & & \downarrow \Pi_h^n & & \\ 0 & \hookrightarrow & V_h^0 & \xrightarrow{\text{curl}} & V_h^{n-1} & \xrightarrow{\text{div}} & V_h^n & \longrightarrow & 0 \end{array} \quad n=2 \quad (3.4b)$$

However, the space C^∞ is too restrictive for our purposes. We therefore extend the domain of Π_h^k to the Hilbert spaces introduced in Sections 2.5.2 and 2.5.3.

Lemma 3.2. *The operator Π_h^k is well-defined on $X^k \cup W_h^k$.*

Proof. First, the space W_h^k consists of nodal VE spaces which are bounded, continuous functions. The evaluation of the degrees of freedom is therefore well-defined for each k .

For X^k , we consider five cases and it is sufficient to consider the local spaces on an element $K \in \mathcal{T}_h$.

- ($k = 0, n = 2$) By Lemma 2.4, $\text{curl } v \in V_h^{n-1}$ implies $(\text{curl } v)|_K \in [H^1(K)]^2$ whereby $v \in H^2(K)$. In turn, $v|_{\partial K} \in H^{3/2}(\partial K)$ which implies that the restriction of v on the skeleton $\bigcup_{F \in \mathcal{F}} F$ is equal to a continuous function in the sense of L^2 . This continuous representative allows us to define a nodal evaluation of v .
- ($k = 0, n = 3$) By Lemma 2.4, $(\text{grad } v)|_K \in V_h^{n-2} \subset [H^1(K)]^3$ so that $v|_K \in H^2(K)$. Applying consecutive trace inequalities gives us $(v|_F)|_{\partial F} \in H^{2-1/2-1/2}(\partial F) = H^1(\partial F)$. In turn, the nodal values of v on the mesh-skeleton are well-defined.

- ($k = n - 2$, $n = 3$) For $v \in X^{n-2}$, we have $\text{curl } v \in V_h^{n-1}$ and, in turn, Lemma 2.4 gives us $\text{curl } v \in [H^1(K)]^3$. Consequently $\int_E v \cdot \vec{t}$ is well-defined, c.f. [14, Prop. 4.5].
- ($k = n - 1$) Since $X^{n-1} \subset W^{n-1}$, each $v \in X^{n-1}$ has a well-defined normal trace $(\vec{n} \cdot v)|_F \in H^{\frac{1}{2}}(F) \subset L^2(F)$ on the mesh facets F .
- ($k = n$) In this case, Π_h^n is the L^2 -projection onto the elementwise constants, which is well-defined on $L^2(\Omega) \supset X^n$.

The evaluation of the degrees of freedom is thus well-defined for both X^k and W_h^k , and so is the interpolant. \square

With the domain of Π_h^* extended from C^∞ , we now prove its most important property in the following lemma.

Lemma 3.3. Π_h^* is a co-chain projection, i.e.

$$\Pi_h^{k+1} d = d \Pi_h^k. \quad (3.5)$$

Proof. Again, the $n = 3$ case was shown in [18] and we focus on $n = 2$. Fix $K \in \mathcal{T}_h$ and let v be a sufficiently regular function to be in the domain of Π_h^k . We divide into cases of $k = 0$ and $k = 1$. By Lemma 3.2 it is enough to show that the degrees of freedom of V_h^{n-1} respectively V_h^n coincide.

- ($k = 0$) Note that for $F \in \mathcal{F}(K)$

$$\text{dof}_F^{n-1}(\Pi_h^{n-1}(\text{curl } v)) = \text{dof}_F^{n-1}(\text{curl } v) = \int_F \vec{n} \cdot (\text{curl } v) = \int_F \vec{t} \cdot \text{grad } v = v(F_1) - v(F_0), \quad (3.6)$$

$$\text{dof}_F^{n-1}(\text{curl}(\Pi_h^0 v)) = \int_F \vec{n} \cdot (\text{curl}(\Pi_h^0 v)) = \int_F \vec{t} \cdot \text{grad}(\Pi_h^0 v) = \Pi_h^0 v(F_1) - \Pi_h^0 v(F_0) = v(F_1) - v(F_0). \quad (3.7)$$

- ($k = 1$) We have

$$\text{dof}_K^n(\Pi_h^n(\text{div } v)) = \text{dof}_K^n(\text{div } v) = \int_K \text{div } v, \quad (3.8)$$

$$\text{dof}_K^n(\text{div}(\Pi_h^{n-1} v)) = \int_K \text{div}(\Pi_h^{n-1} v) = \int_{\partial K} \Pi_h^{n-1} v \cdot \vec{n} = \int_{\partial K} v \cdot \vec{n} = \int_K \text{div } v. \quad (3.9)$$

\square

3.2.1. Exactness of the discrete complex

The combination of the co-chain projection Π_h^k with the regular decomposition of V^k from Section 2.4 now allow us to prove that (V_h^*, d) is exact. While this result was shown in [15] for $n = 3$, we present it here as an alternative proof.

Theorem 3.4. (V_h^*, d) is an exact co-chain complex, i.e.

$$dV_h^k = \ker_d(V_h^{k+1}). \quad (3.10)$$

Proof. The inclusion $dV_h^k \subseteq \ker_d(V_h^{k+1})$ was shown in Lemma 3.1 so we proceed to prove the converse inclusion. Let $v_h \in V_h^{k+1}$ with $dv_h = 0$. Since $V_h^{k+1} \subset V^k$, the exactness of (V^*, d) implies that a $u \in V^k$ exists with $du = v_h$. The regular decomposition from Lemma 2.3 then guarantees that $\psi \in W^k$ and $p \in V^{k-1}$ exist such that $u = \psi + dp$. In turn, we derive that $d\psi = d(u - dp) = v_h$ and thus $\psi \in X^k$. Let us now set $u_h := \Pi_h^k \psi \in V_h^k$, which is well-defined by Lemma 3.2. Using the commuting property of Lemma 3.3, we obtain

$$du_h = d\Pi_h^k \psi = \Pi_h^{k+1} d\psi = \Pi_h^{k+1} v_h = v_h. \quad (3.11)$$

Thus, we have shown that $\ker_d(V_h^{k+1}) \subseteq dV_h^k$. \square

Corollary 3.5 (Stable discrete potential). *Given $v_h \in V_h^k$ with $dv_h = 0$, there exists a discrete potential $u_h \in V_h^{k-1}$ such that*

$$du_h = v_h, \quad \|u_h\|_{V^{k-1}} \lesssim \|v_h\|. \quad (3.12)$$

Proof. Due to Theorem 3.4, the result follows directly from Lemma 2.2. \square

3.2.2. Approximation properties for regular functions

In addition to the commuting property, the interpolation operators have optimal approximation properties when applied to sufficiently regular functions. We summarize these as a general result in the following theorem, and outline the details for the edge space in a separate, subsequent lemma.

Theorem 3.6 (Approximation properties). *For $v \in X^k \cup W_h^k$, we have*

$$\|(I - \Pi_h^k)v\| \lesssim h\|v\|_1. \quad (3.13)$$

Proof. Let us consider four cases:

- ($k = 0$) If $v \in W_h^0 = V_h^0$ then $v = \Pi_h^0 v$ and the result is trivial. For $v \in X^0$, we use Lemma 3.3 to observe that $d\Pi^0 v = \Pi^1 dv = dv$. In turn, $(I - \Pi^0)v \in \ker_d(V^0) = \{0\}$ by the exactness of (V^\bullet, d) and we again conclude $v = \Pi^0 v$.
- ($k = n - 2, n = 3$) The result follows from Lemma 3.7, proven below, after summing over all elements K .
- ($k = n - 1$) Since $X^{n-1}(K) \cup W_h^{n-1}(K) \subset W^{n-1}(K)$, the result follows from [14, Prop. 3.2] combined with the convexity assumption (2) from Assumption 2.1.
- ($k = n$) In this case, Π_h^n is the L^2 -projection onto the elementwise constants. The difference $(I - \Pi_h^n)v$ therefore has zero mean on each element K . The result follows from the Poincaré inequality after summing over all $K \in \mathcal{T}_h$.

\square

Lemma 3.7 (Edge interpolant). *For $n = 3$ and $K \in \mathcal{T}_h$, we have*

$$\|(I - \Pi_h^{n-2})v\|_K \lesssim h\|v\|_{1,K}, \quad \forall v \in X^{n-2} \cup W_h^{n-2} \quad (3.14)$$

Proof. Let us divide into two cases depending on if $v \in X^{n-2}(K)$ or $v \in W_h^{n-2}(K)$.

- ($v \in X^{n-2}(K)$) By definition of the X^k spaces, we have $v \in W^{n-2}(K)$ and $\text{curl } v \in V_h^{n-1}$. In turn, Lemma 2.4 gives us $\text{curl } v \in W^{n-1}(K)$. From [14, Prop. 4.5] we therefore have for all $1/2 < s \leq 1$

$$\|(I - \Pi_h^{n-2})v\|_K \lesssim h^s |v|_{s,K} + h\|\text{curl } v\|_K + h^{s+1} |\text{curl } v|_{s,K}. \quad (3.15)$$

Taking $s = 1$ and bounding $\|\text{curl } v\|_K \leq \|v\|_{1,K}$, we get

$$\|(I - \Pi_h^{n-2})v\|_K \lesssim h\|v\|_{1,K} + h^2 |\text{curl } v|_{1,K}. \quad (3.16)$$

Let $w_h := \text{curl } v \in V_h^{n-1}(K) \cap W^{n-1}(K)$. We can invoke [18, Lem. 3] on w_h

$$|w_h|_{s',K} \lesssim h^{-s'} \|w_h\|_K, \quad (3.17)$$

for some $1/2 < s' \leq 1$. This s' is the minimum value for which both of the following statements hold:

- The solution to the Laplace problem with Neumann boundary data $w_h \cdot \vec{n} \in H^{1/2}(\partial K)$ on K is in $H^{s'+1}(K)$.
- The spaces $H^{\text{div}}(K)$ and $H^{\text{curl}}(K)$ are continuously embedded in $H^{s'}(K)$.

By (2) of Assumption 2.1, both statements hold for $s' = 1$, see [21, Thm. 2, Thm. 4, page 16] [20, Cor. 23.5] respectively [1, Prop. 3.7, Cor. 23.5]. Therefore, we can bound the second term:

$$\|(I - \Pi_h^{n-2})v\|_K \lesssim h\|v\|_{1,K} + h^2|\operatorname{curl} v|_{1,K} \lesssim h\|v\|_{1,K} + h\|\operatorname{curl} v\|_K \lesssim h\|v\|_{1,K}. \quad (3.18)$$

- ($v \in W_h^{n-2}(K)$) Let $\bar{v} \in V_h^{n-2}(K)$ be the mean of v over K . Then by the Poincaré inequality

$$\|(I - \Pi_h^{n-2})v\|_K \leq \|v - \bar{v}\|_K + \|\bar{v} - \Pi_h^{n-2}v\|_K \lesssim h|v|_{1,K} + \|\bar{v} - \Pi_h^{n-2}v\|_K. \quad (3.19)$$

We estimate the second term. The interpolant preserves constants, so $\Pi_h^{n-2}\bar{v} = \bar{v}$. We now use [14, Cor. 4.3], the definition of the edge interpolant as an L^2 -projection on edges, VEM trace inequalities in 2D (2.28a) and 3D (2.28b), and a Poincaré inequality:

$$\begin{aligned} \|\bar{v} - \Pi_h^{n-2}v\|_K &= \|\Pi_h^{n-2}(\bar{v} - v)\|_K \lesssim h \sum_{F \in \mathcal{F}(K)} \sum_{E \in \mathcal{E}(F)} \|\Pi_h^{n-2}(\bar{v} - v) \cdot \vec{t}\|_E \\ &\leq h \sum_{F \in \mathcal{F}(K)} \sum_{E \in \mathcal{E}(F)} \|(\bar{v} - v) \cdot \vec{t}\|_E \\ &\lesssim h^{1/2} \sum_{F \in \mathcal{F}(K)} \|\bar{v} - v\|_F \lesssim \|\bar{v} - v\|_K \lesssim h|v|_{1,K}. \end{aligned} \quad (3.20)$$

The combination of (3.19) and (3.20) yields the result. \square

3.2.3. Stability of the co-chain projection

A direct consequence of the approximation property Theorem 3.6, is that the interpolation operators are stable.

Corollary 3.8 (Stability in the L^2 -norm). *For $v \in X^k \cup W_h^k$, we have*

$$\|\Pi_h^k v\| \lesssim \|v\|_1. \quad (3.21)$$

Proof. An application of the triangle inequality with Theorem 3.6 leads us to

$$\|\Pi_h^k v\| \leq \|\Pi_h^k v - v\| + \|v\| \lesssim h\|v\|_1 + \|v\|_1 \lesssim \|v\|_1. \quad \square$$

Remark 3.1. For $k = n$, we recall that Π_h^n is an L^2 -projection onto the piecewise constants, which is even stable in L^2 , i.e. $\|\Pi_h^n v\| \lesssim \|v\|$ for all $v \in V^n$.

However, we require a slightly stronger result in our analysis. Let us therefore focus on the auxiliary nodal spaces W_h^k and consider stability of Π_h^k in the V^k -norm.

Theorem 3.9 (Stability in the V^k -norm). *For $v \in W_h^k$,*

$$\|\Pi_h^k v\|_{V^k} \lesssim \|v\|_1. \quad (3.22)$$

Proof. By Corollary 3.8 it suffices to prove $\|d\Pi_h^k v\| \lesssim \|v\|_1$. We consider four cases:

- ($k = 0$) Since $W_h^0 = V_h^0$, we have that $\Pi_h^0 W_h^0 = W_h^0$. Thus, $\|d\Pi_h^0 v\| = \|dv\| \leq \|v\|_1$ for $v \in W_h^0$.
- ($k = n - 2, n = 3$) Fix $K \in \mathcal{T}_h$ and let $w \in W_h^{n-2}(K)$ and consider $v = w - \bar{w}$, in which \bar{w} is the mean of w on K . Since $\Pi_h^{n-2}\mathbb{P}_0(K)^3 = \mathbb{P}_0(K)^3$, we have

$$\operatorname{curl} \Pi_h^{n-2} w = \operatorname{curl} \Pi_h^{n-2} v + \operatorname{curl} \Pi_h^{n-2} \Pi_K^n w = \operatorname{curl} \Pi_h^{n-2} v. \quad (3.23)$$

We continue by bounding the norm on the right-hand side. The commuting property from Lemma 3.3 and [14, Prop. 3.1] give us

$$\|\operatorname{curl} \Pi_h^{n-2} v\|_K = \|\Pi_h^{n-1} \operatorname{curl} v\|_K \lesssim h^{\frac{1}{2}} \|\tilde{\mathbf{n}} \cdot (\Pi_h^{n-1} \operatorname{curl} v)\|_{\partial K} = h^{\frac{1}{2}} \sum_{F \in \mathcal{F}(K)} \|\tilde{\mathbf{n}} \cdot (\Pi_h^{n-1} \operatorname{curl} v)\|_F \quad (3.24)$$

The operator Π_h^{n-1} takes the mean of the normal component on each face. Since $v \in W_h^{n-2}$, v is linear on each edge, and this leads us to

$$\begin{aligned} \tilde{\mathbf{n}} \cdot (\Pi_h^{n-1} \operatorname{curl} v)|_F &= \frac{1}{|F|} \int_F \tilde{\mathbf{n}} \cdot (\operatorname{curl} v) = \frac{1}{|F|} \int_F \operatorname{div}_F(\tilde{\mathbf{n}} \times v) = \frac{1}{|F|} \int_{\partial F} \tilde{\mathbf{t}} \cdot v = \sum_{e \in \mathcal{E}(F)} \frac{|e|}{|F|} \sum_{n \in \mathcal{N}(e)} \frac{\tilde{\mathbf{t}}_e \cdot v(n)}{2} \\ &\lesssim h^{-1} \sum_{n \in \mathcal{N}(F)} |v(n)|. \end{aligned}$$

This gives us the following bound on the norm on F :

$$\|\tilde{\mathbf{n}} \cdot (\Pi_h^{n-1} \operatorname{curl} v)\|_F \lesssim \left(h^{-1} \sum_{n \in \mathcal{N}(F)} |v(n)| \right) \|1\|_F \lesssim \sum_{n \in \mathcal{N}(F)} |v(n)|.$$

Using this bound on (3.24) and [23, Thm. 4.2], we obtain the estimate

$$\|\operatorname{curl} \Pi_h^{n-2} v\|_K \lesssim h^{\frac{1}{2}} \sum_{n \in \mathcal{N}(K)} |v(n)| \lesssim h^{\frac{1}{2}} \left(\sum_{n \in \mathcal{N}(K)} |v(n)|^2 \right)^{\frac{1}{2}} \lesssim h^{-1} \|v\|_K \quad (3.25)$$

Finally, we recall that v has zero mean by definition. Hence, the Poincaré inequality can be invoked, giving us

$$\|\operatorname{curl} \Pi_h^{n-2} w\|_K = \|\operatorname{curl} \Pi_h^{n-2} v\|_K \lesssim |v|_{1,K} = |w|_{1,K}. \quad (3.26)$$

Summing (3.26) over all elements $K \in \mathcal{T}_h$, we obtain the result.

- ($k = n - 1$) We have to prove that $\|\operatorname{div} \Pi_h^{n-1} v\| \lesssim \|v\|_1$. We proceed by making use of the commuting property from Lemma 3.3 and Remark 3.1,

$$\|\operatorname{div} \Pi_h^{n-1} v\| = \|\Pi_h^n \operatorname{div} v\| \leq \|\operatorname{div} v\| \leq \|v\|_1. \quad (3.27)$$

- ($k = n$) Since $dv = 0$, the result follows directly from Corollary 3.8. □

3.3. Clément interpolation operator for virtual elements

We continue by constructing an additional interpolation operator that maps to the nodal spaces W_h^k . Let $\Theta_h^0 : H^1(\Omega) \rightarrow V_h^0$ denote the Clément type interpolation operator introduced in [12]. Let now Θ_h^k be the operator acting on $v \in W^k = [H^1(\Omega)]^{\binom{n}{k}}$ by applying Θ_h^0 component-wise. Then

$$\Theta_h^k : W^k \rightarrow W_h^k \quad (3.28)$$

and its properties are shown in the following lemma.

Lemma 3.10 (Clément interpolant). *Boundary conditions are preserved in the sense that $\Theta_h^k [H_0^1(\Omega)]^{\binom{n}{k}} \subset [H_0^1(\Omega)]^{\binom{n}{k}}$ and*

$$\|(I - \Theta_h^k) v\| \lesssim h \|v\|_1, \quad \|\Theta_h^k v\|_1 \lesssim \|v\|_1, \quad \forall v \in W^k. \quad (3.29)$$

Proof. We prove the lemma for Θ_h^0 , since the proof for Θ_h^k follows by applying the arguments componentwise. The following properties were shown in [12, Thm. 11]:

$$\|(I - \Theta_h^0)v\| + h|(I - \Theta_h^0)v|_1 \lesssim h\|v\|_1, \quad \Theta_h^0 H_0^1(\Omega) \subset H_0^1(\Omega). \quad (3.30)$$

This immediately provides the interpolation estimate $\|(I - \Theta_h^0)v\| \lesssim h\|v\|_1$. Moreover, (3.30) implies $|(I - \Theta_h^0)v|_1 \lesssim \|v\|_1$ and combined with a triangle inequality, we thus obtain stability:

$$\|\Theta_h^0 v\|_1 \lesssim \|v\|_1 + \|(I - \Theta_h^0)v\|_1 \lesssim \|v\|_1. \quad (3.31)$$

□

3.4. The main result

With the results presented in the previous subsections, we are now ready to prove the main result of this paper, namely the regular decomposition of VE spaces of lowest order.

Theorem 3.11 (Virtual element regular decomposition). *Given $v_h \in V_h^k$, there exist functions $\tilde{v}_h \in V_h^k$, $\psi_h \in W_h^k$, and $p_h \in V_h^{k-1}$ such that*

$$v_h = \tilde{v}_h + \Pi_h^k \psi_h + dp_h. \quad (3.32a)$$

Moreover, the decomposition is stable in the following sense:

$$\|h^{-1}\tilde{v}_h\| + \|\psi_h\|_1 \lesssim \|dv_h\|, \quad \|p_h\|_{V^{k-1}} \lesssim \|v_h\|_{V^k}. \quad (3.32b)$$

Proof. We follow [22]. First, we use the continuous regular decomposition of Lemma 2.3 to write $v_h = \psi + dp$ with $\psi \in W^k$ and $p \in V^{k-1}$ satisfying

$$\|\psi\|_1 \lesssim \|dv_h\|, \quad \|p\|_{V^{k-1}} \lesssim \|v_h\|_{V^k}. \quad (3.33a)$$

Note that $d\psi = d(v_h - dp) = dv_h \in V_h^{k+1}$ and so $\psi \in X^k$. By Lemma 3.2, $\Pi_h^k \psi$ is then well-defined. Using the co-chain projection property from Lemma 3.3, it follows that

$$d(I - \Pi_h^k)\psi = (I - \Pi_h^{k+1})d\psi = (I - \Pi_h^{k+1})dv_h = 0. \quad (3.34)$$

Now the exactness of the continuous complex implies the existence of a $q \in V^{k-1}$ such that $dq = (I - \Pi_h^k)\psi$. Let us consider the following decomposition of ψ :

$$\psi = \underbrace{\Pi_h^k(\psi - \Theta_h^k \psi)}_{\in V_h^k} + \underbrace{\Pi_h^k \Theta_h^k \psi}_{\in W_h^k} + \underbrace{(I - \Pi_h^k)\psi}_{=dq \in \ker_d(V^k)}. \quad (3.35)$$

We set $\tilde{v}_h := \Pi_h^k(\psi - \Theta_h^k \psi)$ and $\psi_h := \Pi_h^k \Theta_h^k \psi$. In order to define p_h , we first make the following observation:

$$d(p + q) = v_h - \psi + (I - \Pi_h^k)\psi = v_h - \Pi_h^k \psi \in V_h^k. \quad (3.36)$$

Corollary 3.5 now provides $p_h \in V_h^{k-1}$ with $dp_h = d(p + q)$ and $\|p_h\|_{V^k} \lesssim \|d(p + q)\|$.

The decomposition (3.32a) now follows by construction, since

$$\tilde{v}_h + \Pi_h^k \psi_h + dp_h = \Pi_h^k(\psi - \Theta_h^k \psi) + \Pi_h^k \Theta_h^k \psi + v_h - \Pi_h^k \psi = v_h. \quad (3.37)$$

We continue by proving the bounds for each component. First, by the approximation estimates of Theorem 3.6 and Lemma 3.10, we derive

$$\begin{aligned} \|h^{-1}\tilde{v}_h\| &= \|h^{-1}\Pi_h^k(\psi - \Theta_h^k\psi)\| \leq \|h^{-1}(I - \Theta_h^k)\psi\| + \|h^{-1}(I - \Pi_h^k)\underbrace{(I - \Theta_h^k)\psi}_{\in X^k + W_h^k}\| \\ &\lesssim \|\psi\|_1 + \|(I - \Theta_h^k)\psi\|_1 \leq 2\|\psi\|_1 + \|\Theta_h^k\psi\|_1 \lesssim \|\psi\|_1 \lesssim \|dv_h\|, \end{aligned} \quad (3.38a)$$

in which the second-to-last inequality is due to the stability of Θ_h^k (Lemma 3.10), and the last follows from (3.33a). These last inequalities also allow us to bound

$$\|\psi_h\| = \|\Theta_h^k\psi\| \lesssim \|\psi\|_1 \lesssim \|dv_h\|. \quad (3.38b)$$

Finally, the definition of p_h combined with Theorem 3.6 and (3.33a) results in

$$\|p_h\|_{V^{k-1}} \lesssim \|d(p+q)\| \leq \|dp\| + \|dq\| = \|dp\| + \|(I - \Pi_h^k)\psi\| \lesssim \|dp\| + h\|\psi\|_1 \lesssim \|v_h\|_{V^k}. \quad (3.38c)$$

Together, (3.38) forms (3.32b). \square

By applying the regular decomposition from Theorem 3.11 twice, we obtain a further decomposition that consists solely of *regular* functions in the nodal spaces, e.g. $\psi_h \in W_h^k$, and *high-frequency* functions, e.g. $\tilde{v}_h \in V_h^k$ for which $\|h^{-1}\tilde{v}_h\|$ is bounded.

Corollary 3.12 (Deeper decomposition). *Given $v_h \in V_h^k$, there exist functions $\tilde{v}_h \in V_h^k$, $\psi_h \in W_h^k$, and $\tilde{p}_h \in V_h^{k-1}$, $\phi_h \in W_h^{k-1}$ such that*

$$v_h = \tilde{v}_h + \Pi_h^k\psi_h + d\tilde{p}_h + d\Pi_h^{k-1}\phi_h, \quad (3.39a)$$

and

$$\|h^{-1}\tilde{v}_h\| + \|\psi_h\|_1 \lesssim \|dv_h\|, \quad \|h^{-1}\tilde{p}_h\| + \|\phi_h\|_1 \lesssim \|v_h\|_{V^k}. \quad (3.39b)$$

Proof. We first apply Theorem 3.11 to decompose $v_h = \tilde{v}_h + \Pi_h^k\psi_h + dp_h$. We now apply Theorem 3.11 again on $p_h \in V_h^{k-1}$ to get

$$p_h = \tilde{p}_h + \Pi_h^{k-1}\phi_h + dq_h, \quad (3.40)$$

where $\tilde{p}_h \in V_h^{k-1}$, $\phi_h \in W_h^{k-1}$ and $q_h \in V_h^{k-2}$. Substituting the definitions and using $dd = 0$, we obtain

$$\begin{aligned} v_h &= \tilde{v}_h + \Pi_h^k\psi_h + d(\tilde{p}_h + \Pi_h^{k-1}\phi_h + dq_h) \\ &= \tilde{v}_h + \Pi_h^k\psi_h + d\tilde{p}_h + d\Pi_h^{k-1}\phi_h, \end{aligned} \quad (3.41)$$

which is exactly (3.39a). The bounds on \tilde{v}_h and ψ_h now follow from Theorem 3.11. Similarly, we obtain:

$$\|h^{-1}\tilde{p}_h\| + \|\phi_h\|_1 \lesssim \|dp_h\| \lesssim \|v_h\|_{V^k}. \quad (3.42)$$

\square

4. AUXILIARY SPACE PRECONDITIONING

We now aim to use the regular decomposition from Section 3.4 to construct an efficient numerical solver using the framework of auxiliary space preconditioning [22]. After introducing the framework in Section 4.1, we apply it to the VE spaces in Section 4.2. Finally, Section 4.3 briefly shows a multiplicative variant of the preconditioner.

4.1. Abstract framework

In this exposition, we closely follow [22]. First, let V be a Hilbert space with inner product $(\cdot, \cdot)_V$, norm $\|\cdot\|_V$ and dual space V' . Let $A : V \rightarrow V'$ be the linear operator associated to the inner product, i.e.

$$\langle Au, v \rangle_{V' \times V} = (u, v)_V, \quad \langle Au, v \rangle_{V' \times V} = \|v\|_V^2, \quad \forall u, v \in V. \quad (4.1)$$

Second, let $S : V \rightarrow V'$ be a symmetric, positive definite, linear operator. In turn, S induces an additional norm on V :

$$\|v\|_S := \langle Sv, v \rangle_{V' \times V}^{\frac{1}{2}} \quad \forall v \in V. \quad (4.2)$$

We assume that S is easily invertible and refer to the application of S^{-1} as the *smoother*.

Third, let the *auxiliary spaces* W_j be Hilbert spaces for $j = 1, 2, \dots, J$. Analogous to (4.1), we let $A_j : W_j \rightarrow W'_j$ be the linear operator associated with the inner product on W_j . We furthermore equip each W_j with a continuous and linear *transfer operator* $\pi_j : W_j \rightarrow V$, whose adjoint is denoted by $\pi_j^* : V' \rightarrow W'_j$.

Then the abstract auxiliary space preconditioner $B : V' \rightarrow V$ is defined as:

$$B := S^{-1} + \sum_{j=1}^J \pi_j A_j^{-1} \pi_j^*. \quad (4.3)$$

Theorem 4.1 (Auxiliary space preconditioner). *Let $v \in V, w_j \in W_j, j = 1, \dots, J$. If the following three conditions hold:*

(1) *The smoother S^{-1} is continuous:*

$$\|v\|_V \leq c_s \|v\|_S, \quad c_s > 0. \quad (4.4a)$$

(2) *The transfer functions π_j are continuous for all $j = 1, \dots, J$:*

$$\|\pi_j w_j\|_V \leq c_j \|w_j\|_{W_j}, \quad c_j > 0. \quad (4.4b)$$

(3) *For every $v \in V$, there exist $v_0 \in V$ and $w_j \in W_j$ such that*

$$v = v_0 + \sum_{j=1}^J \pi_j w_j, \quad \|v_0\|_S^2 + \sum_{j=1}^J \|w_j\|_{W_j}^2 \leq c_0 \|v\|_V^2, \quad c_0 > 0. \quad (4.4c)$$

Then, for B given by (4.3), the spectral condition number of the preconditioned system BA is bounded;

$$\kappa(BA) := \frac{\lambda_{\max}(BA)}{\lambda_{\min}(BA)} \leq c_0^2 \left(c_s^2 + \sum_{j=1}^J c_j^2 \right). \quad (4.5)$$

Proof. See the proof of [22, Thm. 2.2] and the remarks around [22, (2.6) and (2.14)]. \square

4.2. Virtual element auxiliary space preconditioners

Before we construct the nodal auxiliary space preconditioners according to Theorem 4.1, we note that preconditioning the operator A on V_h^k is not necessary for all k . In particular:

- If $k = 0$, the decomposition of Theorem 4.1 is trivial since $W_h^0 = V_h^0$ and so we may set $\psi_h = v_h$. In this case a multi-grid method is applicable, see e.g. [2].
- For $k = n$, we have $V_h^n = \mathbb{P}_0$ and so the operator A is diagonal and no preconditioner is necessary.

We therefore focus on the remaining cases of $0 < k < n$. Section 4.2.1 introduces the smoother and the particular constructions for $k = 1, 2$ are considered in Sections 4.2.2 and 4.2.3, respectively.

4.2.1. A virtual element smoother

Due to the discussion in the previous subsection, we only need to define the smoother for $0 < k < n$. We propose two alternatives. First, given v_h , let $\sum_i v_{h,i}$ be its decomposition such that each $v_{h,i}$ is a scaled basis function of V_h^k . We then define the diagonal operator

$$\|v_h\|_{D^k}^2 = \langle D^k v_h, v_h \rangle = \sum_i \|v_{h,i}\|_{V^k}^2. \quad (4.6)$$

Second, recalling Lemma 2.7 we propose using the stabilization term common to VEM:

$$\|v_h\|_{S^k}^2 = \langle S^k v_h, v_h \rangle = \sum_{K \in \mathcal{T}_h} \|h^{-1} v_h\|_{S^k, K}^2, \quad (4.7a)$$

$$\|v_h\|_{S^k, K}^2 = \begin{cases} h \sum_{F \in \mathcal{F}(K)} (v_h \cdot \vec{n}, v_h \cdot \vec{n})_F, & (k = n-1) \\ h^2 \sum_{E \in \mathcal{E}(K)} (v_h \cdot \vec{t}, v_h \cdot \vec{t})_E, & (k = n-2; n=3) \end{cases} \quad (4.7b)$$

Note that (4.7b) corresponds to the VEM stabilization operator defined in [14, (54), (58), (73)]. Recall that the decompositions from Theorem 3.11 and Corollary 3.12 include high-frequency terms that are bounded in norms weighted by h^{-1} . In order to make the connection between these terms and the smoother (4.7a), we present the following lemma.

Lemma 4.2 (Two smoothers). *For $0 < k < n$, the operators D^k and S^k induce norms on V_h^k that satisfy*

$$\|v_h\|_{V^k} \lesssim \|v_h\|_{D^k} \lesssim \|v_h\|_{S^k} \lesssim \|h^{-1} v_h\|, \quad \forall v_h \in V_h^k. \quad (4.8)$$

Proof. We prove the three bounds separately.

- (1) We follow [22, (7.2)]. We have for any $v_h \in V_h^k$ that the square of its energy norm can be computed by summing squares of local contributions;

$$\|v_h\|_{V^k}^2 = \sum_{K \in \mathcal{T}_h} \left\| \sum_i v_{h,i} \right\|_{V^k, K}^2 \leq \sum_{K \in \mathcal{T}_h} N_K \sum_i \|v_{h,i}\|_{V^k, K}^2 \leq \max_{K \in \mathcal{T}_h} N_K \|v_h\|_{D^k}^2, \quad (4.9)$$

by the Cauchy-Schwartz inequality. Here N_K is the number of basis functions whose support overlaps with K .

- (2) For the part involving only the L^2 -norm of v_h , Lemma 2.7 gives us

$$\sum_i \|v_{h,i}\|^2 \approx \sum_i \sum_{K \in \mathcal{T}_h} \|v_{h,i}\|_{S^k, K}^2 = \sum_{K \in \mathcal{T}_h} \sum_i \|v_{h,i}\|_{S^k, K}^2 = \sum_{K \in \mathcal{T}_h} \|v_h\|_{S^k, K}^2 \lesssim \sum_{K \in \mathcal{T}_h} \|h^{-1} v_h\|_{S^k, K}^2 = \|v_h\|_{S^k}^2$$

It remains to show that $\sum_i \|dv_{h,i}\|^2 \lesssim \|v_h\|_{S^k}^2$. We distinguish two cases

- ($k = n-1$) Let us rewrite $v_{h,i} = \alpha_i b_{h,i}$ with $\alpha_i \in \mathbb{R}$ and $b_{h,i}$ a basis function of V_h^k . On an element K in the support of $b_{h,i}$, we compute:

$$\begin{aligned} \|dv_{h,i}\|_K^2 &= \alpha_i^2 \|\operatorname{div} b_{h,i}\|_K^2 = \alpha_i^2 |K|^{-1} \approx \alpha_i^2 h^{-1} |F_i|^{-1} \\ &= \alpha_i^2 h^{-1} \|\vec{n} \cdot b_{h,i}\|_{F_i}^2 = h^{-1} \|\vec{n} \cdot v_{h,i}\|_{F_i}^2 = h^{-1} \|\vec{n} \cdot v_h\|_{F_i}^2 \end{aligned} \quad (4.10)$$

Summing over all basis functions and all elements, we obtain

$$\sum_i \|dv_{h,i}\|^2 \approx \sum_i h^{-1} \|\vec{n} \cdot v_h\|_{F_i}^2 \lesssim \sum_{K \in \mathcal{T}_h} h^{-2} \|v_h\|_{S^k, K}^2 = \|v_h\|_{S^k}^2 \quad (4.11)$$

- ($k = n - 2$, $n = 3$) Let again $v_{h,i} = \alpha_i b_{h,i}$. Then

$$\begin{aligned} \|dv_{h,i}\|_K^2 &= \alpha_i^2 \|\operatorname{curl} b_{h,i}\|_K^2 \approx \alpha_i^2 \|\operatorname{curl} b_{h,i}\|_{S^{n-1},K}^2 = \sum_{F \in \mathcal{F}(E_i)} h \alpha_i^2 \|\vec{n} \cdot \operatorname{curl} b_{h,i}\|_F^2 \\ &= \sum_{F \in \mathcal{F}(E_i)} h \alpha_i^2 \|\operatorname{div}_F(\vec{n} \times b_{h,i})\|_F^2 \end{aligned} \quad (4.12)$$

From the definition of the edge space V_h^{n-2} , it follows that $\operatorname{div}_F(\vec{n} \times b_{h,i}) \in \mathbb{P}_0(F)$. In particular, we note that

$$\operatorname{div}_F(\vec{n} \times b_{h,i}) = \frac{1}{|F|} \int_F \operatorname{div}_F(\vec{n} \times b_{h,i}) = \frac{1}{|F|} \int_{\partial F} \vec{t} \cdot b_{h,i} = \frac{1}{|F|} \int_{E_i} \vec{t} \cdot b_{h,i} = \frac{\pm 1}{|F|} \quad (4.13)$$

Substituting this in (4.12) leads to

$$\|dv_{h,i}\|_K^2 \approx \sum_{F \in \mathcal{F}(E_i)} h \alpha_i^2 |F|^{-1} \lesssim \alpha_i^2 |E_i|^{-1} = \alpha_i^2 \|\vec{t} \cdot b_{h,i}\|_{E_i}^2 = \|\vec{t} \cdot v_{h,i}\|_{E_i}^2 = h^{-2} \|v_{h,i}\|_{S^k,K}^2 \quad (4.14)$$

Finally, we sum over all elements and basis functions to obtain

$$\sum_i \|dv_{h,i}\|_K^2 \lesssim \sum_{K \in \mathcal{T}_h} h^{-2} \|v_{h,i}\|_{S^k,K}^2 = \sum_{K \in \mathcal{T}_h} h^{-2} \|v_h\|_{S^k,K}^2 = \|v_h\|_{S^k}^2 \quad (4.15)$$

- (3) The final inequality follows from Lemma 2.7.

$$\|v_h\|_{S^k}^2 = \sum_{K \in \mathcal{T}_h} \|h^{-1} v_h\|_{S^k,K}^2 \approx \sum_{K \in \mathcal{T}_h} \|h^{-1} v_h\|_K^2 = \|h^{-1} v_h\|^2 \quad (4.16)$$

□

Lemma 4.2 shows that we have a choice between two smoothers, either D^k or S^k . Moreover, it implies inverse inequalities for the differential operators curl and div applied to the edge respectively facet functions. We summarize this result in the following corollary.

Corollary 4.3 (Edge and facet inverse inequalities). *For the facet and edge virtual element spaces of lowest order, i.e. with $0 < k < n$, the following inverse inequality holds:*

$$\|dv_h\| \lesssim \|h^{-1} v_h\|, \quad \forall v_h \in V_h^k. \quad (4.17)$$

Proof. The result follows from Lemma 4.2, since $\|dv_h\| \leq \|v_h\|_{V^k}$. □

4.2.2. An auxiliary space preconditioner for edge elements

The first case we consider is $k = 1$ with $n = 3$. Given $v_h \in V_h^1$, Theorem 3.11 provides the following decomposition:

$$v_h = \tilde{v}_h + \Pi_h^0 \psi_h + \operatorname{grad} p_h, \quad \|h^{-1} \tilde{v}_h\|^2 + \|\psi_h\|_1^2 + \|p_h\|_1^2 \lesssim \|v_h\|_{V^1}^2. \quad (4.18)$$

Thus, we are led to define the following auxiliary spaces with corresponding inner products and transfer operators:

$$W_1 := W_h^1, \quad \langle A_1 \psi_h, \psi_h \rangle = \|\psi_h\|_1^2, \quad \pi_1 := \Pi_h^1 : W_h^1 \rightarrow V_h^1, \quad (4.19a)$$

$$W_2 := W_h^0 = V_h^0, \quad \langle A_2 p_h, p_h \rangle = \|p_h\|_1^2, \quad \pi_2 := \operatorname{grad} : V_h^0 \rightarrow V_h^1. \quad (4.19b)$$

Theorem 4.4. *Let A denote the operator associated with the inner product of V_h^1 and let*

$$B = (S^1)^{-1} + \Pi_h^1 A_1^{-1} (\Pi_h^1)^* + \operatorname{grad} A_2^{-1} \operatorname{grad}^* \quad (4.20)$$

then the spectral condition number $\kappa(BA)$ is bounded, independent of the mesh size h .

Proof. We verify the three conditions of Theorem 4.1.

- (1) Continuity of the smoother was shown in Lemma 4.2.
- (2) The transfer operator $\Pi_h^1 : W_h^1 \rightarrow V_h^1$ is continuous due to Theorem 3.9. Since the second transfer operator is a differential $d : V_h^{k-1} \rightarrow V_h^k$, its continuity follows from the fact that $dd = 0$:

$$\|dp_h\|_{V^k} = \|dp_h\| \leq \|p_h\|_{V^{k-1}}, \quad \forall p_h \in V_h^{k-1}. \quad (4.21)$$

- (3) The decomposition is given by Theorem 3.11. For the stability of the decomposition, we only need to show that $\|\tilde{v}_h\|_{S^1} \lesssim \|h^{-1}\tilde{v}_h\|$, which was proven in Lemma 4.2 (last inequality).

The robustness with respect to h follows from the fact that the constants c_i with $i \in \{s, 0, 1, 2\}$ are independent of h . \square

Remark 4.1 (Two-dimensional facet elements). *The only difference for $n = 2$ and $k = 1$, is that Π_2 needs to be redefined as $\text{curl} : V_h^0 \rightarrow V_h^1$. With this minor adjustment, the analogue of Theorem 4.1 follows in the same manner.*

4.2.3. An auxiliary space preconditioner for facet elements in 3D

Given $v_h \in V_h^2$ with $n = 3$, Corollary 3.12 provides the following decomposition:

$$v_h = \tilde{v}_h + \Pi_h^2 \psi_h + \text{curl } \tilde{p}_h + \text{curl } \Pi_h^1 \phi_h, \quad \|h^{-1}\tilde{v}_h\|^2 + \|\psi_h\|_1^2 + \|h^{-1}\tilde{p}_h\|^2 + \|\phi_h\|_1^2 \lesssim \|v_h\|_{V^2}^2. \quad (4.22)$$

Thus, we are led to define the following auxiliary spaces, inner products and transfer operators:

$$W_1 := W_h^2, \quad \langle A_1 \psi_h, \psi_h \rangle = \|\psi_h\|_1^2, \quad \pi_1 := \Pi_h^2 : W_h^2 \rightarrow V_h^2, \quad (4.23a)$$

$$W_2 := V_h^1, \quad \langle A_2 \tilde{p}_h, \tilde{p}_h \rangle = \|\tilde{p}_h\|_{S^1}^2, \quad \pi_2 := \text{curl} : V_h^1 \rightarrow V_h^2, \quad (4.23b)$$

$$W_3 := W_h^1, \quad \langle A_3 \phi_h, \phi_h \rangle = \|\phi_h\|_1^2, \quad \pi_3 := \text{curl } \Pi_h^1 : W_h^1 \rightarrow V_h^2. \quad (4.23c)$$

Theorem 4.5. *For $n = 3$, let A denote the operator associated with the inner product of V_h^2 and let*

$$B = (S^2)^{-1} + \Pi_h^2 A_1^{-1} (\Pi_h^2)^* + \text{curl} \left((S^1)^{-1} + \Pi_h^1 A_3^{-1} (\Pi_h^1)^* \right) \text{curl}^* \quad (4.24)$$

then the spectral condition number $\kappa(BA)$ is bounded, independent of the mesh size h .

Proof. We verify the three conditions of Theorem 4.1.

- (1) Continuity of the smoother S^2 was shown in Lemma 4.2.
- (2) The transfer operators $\Pi_h^k : W_h^k \rightarrow V_h^k$ are continuous due to Theorem 3.9, so Π_1 is continuous. For Π_2 , we use the continuity of the curl (4.21) combined with Lemma 4.2 to obtain

$$\|\Pi_2 \tilde{p}_h\|_{V^2} = \|\text{curl } \tilde{p}_h\|_{V^2} = \|\text{curl } \tilde{p}_h\| \leq \|\tilde{p}_h\|_{V^1} \lesssim \|\tilde{p}_h\|_{S^1} \quad (4.25)$$

Finally, the continuity of Π_3 follows by combining Theorem 3.9 with (4.21).

- (3) The decomposition is given by Corollary 3.12. Again, the stability of the decomposition follows from $\|\tilde{v}_h\|_{S^2} \lesssim \|h^{-1}\tilde{v}_h\|$, shown in Lemma 4.2.

Since the constants c_i with $i \in \{s, 0, 1, 2, 3\}$ are independent of h , the preconditioner is robust. \square

4.3. A multiplicative variant

The preconditioners in Theorem 4.4 and Theorem 4.5 can be seen as *additive* preconditioners. A *multiplicative* variant of these operators can be constructed as follows. For a given residual r_0 , we first apply the smoother to create $z_0 \in V_h^k$:

$$z_0 = S^{-1} r_0. \quad (4.26a)$$

Then for each $j \in \{1, \dots, J\}$, we apply the following steps sequentially:

$$r_j = r_{j-1} - Az_{j-1} \quad (4.26b)$$

$$z_j = z_{j-1} + \pi_j A_j^{-1} \pi_j^* r_j \quad (4.26c)$$

Recall that A is the operator from (4.1). Finally, the multiplicative variant of the preconditioner outputs $z_j \in V_h^k$.

5. NUMERICAL EXPERIMENTS

In this section, we present numerical experiments to illustrate the performance of auxiliary space preconditioning for virtual element discretizations of the H^{div} projection problem (2.4) and the Darcy problem (2.6) in 2D.

The experiments are performed in the open source Julia-based virtual element library VirtuE and the run scripts are available at [7]. The numerical experiments are performed on a laptop with an Intel Core i7-8565U CPU and 16 GB of RAM. Throughout our tests we will use D^k of Lemma 4.2 as the smoother in the auxiliary space preconditioner. In our experiments, its performance was better in all cases compared to the smoother S^k obtained from the stabilization term. We will refer to the additive preconditioner from Remark 4.1 as B_{add} and the multiplicative variant from Section 4.3 as B_{mult} .

For each problem, we compare the condition numbers and the performance of GMRES (without restarts) for the original problem $Av = b$ against the preconditioned system $BAv = Bb$. We will conduct two types of numerical experiments. The first tests the robustness of the preconditioner with respect to the mesh size derived in Section 4, whereas the second ventures outside the theory to investigate the dependence of the preconditioner on element aspect ratios.

5.1. H^{div} projection problem

Let us start by describing the VE discretization of problem (2.4): find $v_h \in V_h^{n-1}$ such that

$$(v_h, w_h)_h + (\text{div } v_h, \text{div } w_h) = (f, w_h), \quad \forall w_h \in V_h^{n-1}. \quad (5.1)$$

Here, $(v_h, w_h)_h$ is the mass matrix of the facet space, assembled according to [9]. The function f on the right-hand side is given by

$$f(x, y) = - \begin{bmatrix} 2\pi \cos(2\pi x) \sin(4\pi y) \\ 4\pi \cos(4\pi y) \sin(2\pi x) \end{bmatrix}. \quad (5.2)$$

The right-hand side is assembled by first projecting w_h to the piecewise linears. We construct the mesh by subdividing a structured, $N \times N$ Cartesian grid into triangles, squares, and pentagons, as illustrated in Figure 2.

The results are shown in Table 5.1, in which A denotes the matrix representation of the left-hand side of (5.1). We see that both in terms of conditions numbers and GMRES iterations, the auxiliary space preconditioned system has essentially constant values, and the smallest values. Most importantly, the number of GMRES iterations is not growing with decreasing mesh size, for both the additive and multiplicative variants.

TABLE 5.1. Performance of the nodal auxiliary space preconditioner on the H^{div} projection problem for varying mesh sizes.

N	#dof	Condition numbers				GMRES iterations			
		A	$\text{diag}(A)^{-1}A$	$B_{\text{add}}A$	$B_{\text{mult}}A$	A	$\text{diag}(A)^{-1}A$	$B_{\text{add}}A$	$B_{\text{mult}}A$
4	312	3.19E03	3.36E03	4.48	9.29	114	24	14	16
8	1200	1.28E04	1.35E04	4.50	9.53	234	121	16	17
16	4704	5.13E04	5.39E04	4.51	9.60	427	220	15	17
32	18624	2.05E05	2.15E05	4.51	9.61	739	350	15	15

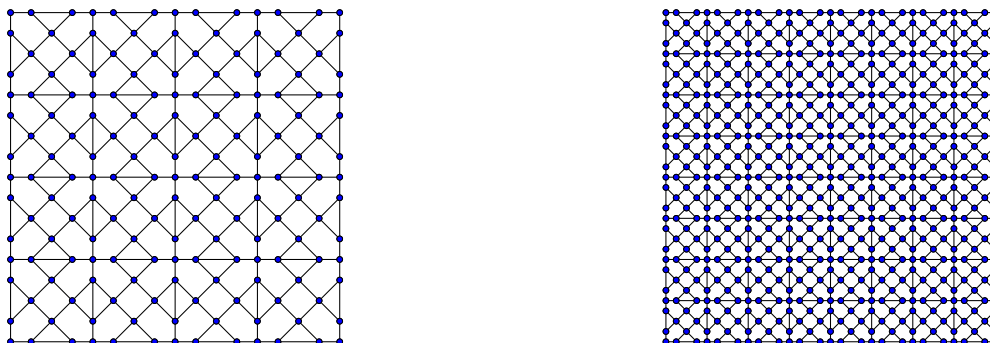


FIGURE 2. The two coarsest meshes (with $N = 4, 8$ respectively) used in the mesh size dependency experiments of Sections 5.1 and 5.2. This sequence of meshes satisfies Assumption 2.1.

5.2. Darcy problem

The discrete Darcy problem reads as follows. Given data $f \in [L^2(\Omega)]^n$ and $g \in L^2(\Omega)$, find $u_h \in V_h^{n-1}$ and $p_h \in V_h^n$ such that

$$(u_h, v_h)_h - (p_h, \operatorname{div} v_h) = (f, v_h), \quad \forall v_h \in V_h^{n-1}, \quad (5.3a)$$

$$-(q_h, \operatorname{div} u_h) = (g, q_h), \quad \forall q_h \in V_h^n. \quad (5.3b)$$

We denote the corresponding system matrix by \mathcal{A} and the mass matrix corresponding to $(u_h, v_h)_h$ by M_u .

Next, we note that (5.3) is well-posed in the product space $H^{\operatorname{div}}(\Omega) \times L^2(\Omega)$. Following the framework of norm-equivalent preconditioning [24], the Riesz representation operator forms a robust preconditioner for this problem. This involves solving an H^{div} projection problem and a projection in L^2 . We therefore construct a block diagonal preconditioner \mathcal{B} where the first block is the nodal auxiliary space preconditioner B and the second block is the inverse of the (diagonal) mass matrix M_p on \mathbb{P}_0 . We compare its performance to a naively constructed preconditioner composed of the diagonal of the mass matrices. Namely, we compare:

$$\mathcal{B} := \begin{bmatrix} B & 0 \\ 0 & M_p^{-1} \end{bmatrix}, \quad \mathcal{B}_{\operatorname{diag}} := \left(\operatorname{diag} \begin{bmatrix} M_u & 0 \\ 0 & M_p \end{bmatrix} \right)^{-1}. \quad (5.4)$$

Let f be as in (5.2) and let $g = -40\pi^2 \cos(2\pi x) \sin(4\pi y)$. We use the same sequence of meshes as depicted in Figure 2 and compare the numbers of iterations for GMRES on the original and preconditioned systems. The results are shown in Table 5.2. The condition numbers of the last iteration are not computed. We note that the number of GMRES iterations is growing with mesh size for the original and diagonal preconditioned systems. In contrast, the auxiliary space preconditioned systems require a stable number of iterations, for both additive and multiplicative variants.

5.3. Aspect ratio tests

In this next experiment, we consider a sequence of meshes on the unit square $\Omega = [0, 1]^2$ induced by a parameter $\epsilon > 0$. For each ϵ , we intersect a background mesh with the line $y = 0.5 + \epsilon$. At each intersection point we create a new vertex and split the adjacent elements, see Figure 3. This example therefore corresponds to a naive remeshing procedure to conform a background mesh to an independently placed, embedded interface. Strictly speaking, this example falls out of the scope of our theory, in particular Assumption 2.1 is violated because the aspect ratios will

TABLE 5.2. Performance of the nodal auxiliary space preconditioner on the Darcy problem for varying mesh sizes. Computation of the condition numbers on the finest grid was not feasible in our implementation and are therefore omitted.

N	#dof	Condition number				GMRES iterations			
		\mathcal{A}	$\mathcal{B}_{\text{diag}}\mathcal{A}$	$\mathcal{B}_{\text{add}}\mathcal{A}$	$\mathcal{B}_{\text{mult}}\mathcal{A}$	\mathcal{A}	$\mathcal{B}_{\text{diag}}\mathcal{A}$	$\mathcal{B}_{\text{add}}\mathcal{A}$	$\mathcal{B}_{\text{mult}}\mathcal{A}$
4	456	3.65E01	7.59E01	3.12	3.21	84	17	29	29
8	1776	1.29E02	1.50E02	3.14	3.27	136	34	34	32
16	7008	5.00E02	2.98E02	3.17	3.29	211	32	35	35
32	27840	-	-	-	-	384	53	35	35

increase as ϵ decreases. We measure the (maximum) aspect ratio of the mesh \mathcal{T}_h by

$$\alpha := \max_{K \in \mathcal{T}_h} \frac{\text{diam}(K)^2}{|K|}. \quad (5.5)$$

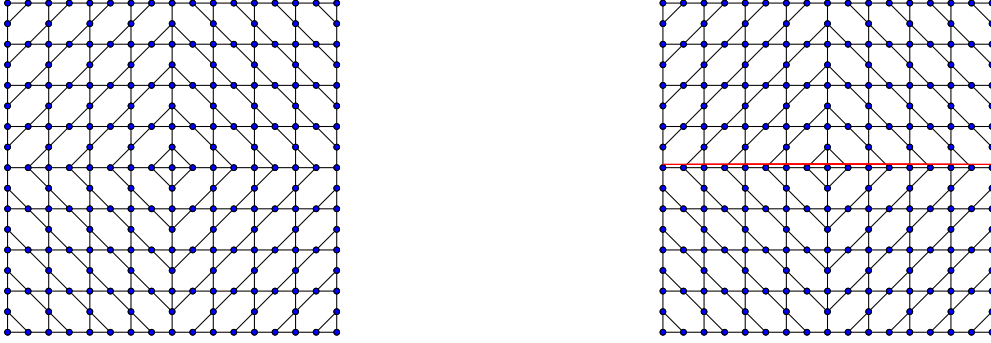


FIGURE 3. Meshes used in the numerical experiments for the aspect ratio tests. The elements crossed by the red line at $y = 0.5 + \epsilon$ are split in two by introducing new nodes at the intersections with mesh edges.

5.3.1. H^{div} projection problem

On the mesh depicted in Figure 2 we solve the H^{div} projection problem with

$$f = \begin{bmatrix} \cos(x) \sinh(y) \\ \sin(x) \cosh(y) \end{bmatrix}, \quad (5.6)$$

and compare the condition number and number of iterations for GMRES on the original and preconditioned systems. The results are shown in Table 5.3. Although the aspect ratio is increasing, the auxiliary space preconditioner performs well, for both additive or multiplicative variants. The number of GMRES iterations is stable and relatively small, and the same holds for the condition numbers.

5.3.2. Darcy problem

Finally, we perform the same aspect ratio experiment for the Darcy problem (5.3). Let here f be as in (5.6) and let $g = 0$. In Table 5.4 we compare the results. As α increases, the number of GMRES iterations increases for the original

TABLE 5.3. H^{div} projection problem: Comparison of the condition numbers and number of iterations for GMRES on the original and preconditioned systems for meshes with increasing aspect ratios.

ϵ	α	Condition numbers				GMRES iterations			
		A	$\text{diag}(A)^{-1}A$	$B_{\text{add}}A$	$B_{\text{mult}}A$	A	$\text{diag}(A)^{-1}A$	$B_{\text{add}}A$	$B_{\text{mult}}A$
-	4.00E00	5.18E03	3.62E03	4.33	11.5	126	116	16	18
1E-2	7.94E00	2.00E04	1.12E04	4.49	13.0	169	204	16	18
1E-4	6.27E02	1.91E06	7.74E05	4.93	11.3	179	270	16	18
1E-6	6.25E04	1.91E08	7.70E07	5.00	11.3	174	275	16	17
1e-8	6.25E06	1.91E10	7.70E09	5.00	11.3	177	159	16	17

and diagonal preconditioned systems, but remains constant for the auxiliary space preconditioned system. This is again true for both additive and multiplicative variants, indicating a promising potential of this approach for general polygonal meshes.

TABLE 5.4. Darcy problem: Comparison of the condition numbers and number of iterations for GMRES on the original and preconditioned systems for meshes with increasing aspect ratios.

ϵ	α	Condition numbers				GMRES iterations			
		\mathcal{A}	$\mathcal{B}_{\text{diag}}\mathcal{A}$	$\mathcal{B}_{\text{add}}\mathcal{A}$	$\mathcal{B}_{\text{mult}}\mathcal{A}$	\mathcal{A}	$\mathcal{B}_{\text{diag}}\mathcal{A}$	$\mathcal{B}_{\text{add}}\mathcal{A}$	$\mathcal{B}_{\text{mult}}\mathcal{A}$
-	4.00E00	4.72E01	9.88E01	3.21	3.29	82	58	32	32
1E-2	7.94E00	8.17E01	1.54E02	3.21	3.29	117	167	36	36
1E-4	6.27E02	8.17E03	2.80E04	3.21	3.31	116	230	35	36
1E-6	6.25E04	8.17E05	2.75E07	3.21	3.31	111	176	35	36
1E-8	6.25E06	1.43E09	2.75E10	3.21	3.31	107	414	34	35

6. CONCLUSION

In this paper, we have formulated and analyzed nodal auxiliary space preconditioners for edge and facet Virtual Element spaces. The preconditioner effectively consists of a series of elliptic problems on nodal VE spaces combined with appropriate smoothers. Our analysis shows that the performance of these preconditioners is independent of the mesh size, which is supported by numerical experiments for the H^{div} projection problem and the Darcy problem, in 2D.

Future research directions on this topic include the following. First, while the theory includes three-dimensional problems, the performance of the preconditioner needs to be verified numerically. Second, the theory can likely be extended to higher-order VE spaces, see e.g. [16], by deriving a regular decomposition of the associated, exact co-chain complex and computing appropriate transfer operators from the higher-order H^1 -conforming VE spaces. Third, the assumptions on the mesh may be weakened, in particular concerning the convexity of the elements, since the numerical experiments indicate a wider applicability. Finally, we note that while the proposed preconditioner involves solving global systems, these solves can be replaced by scalable, spectrally equivalent operators obtained, for example by (algebraic) multi-grid solves. The practical advantages of the resulting preconditioners remain to be investigated.

In conclusion, we have generalized the Hiptmair-Xu nodal auxiliary space preconditioner to the VEM framework. Our numerical results furthermore show promising potential of the preconditioner for problems on meshes with high aspect ratios, obtained by naively adapting a grid to conform to an embedded interface.

The authors warmly thank Lorenzo Mascotto and Lourenco Beirão da Veiga for valuable discussions concerning Lemma 3.7, and Ana Budiša for suggesting the multiplicative variant of the preconditioner (Section 4.3).

REFERENCES

- [1] C. AMROUCHE, C. BERNARDI, M. DAUGE, AND V. GIRAULT, *Vector potentials in three-dimensional non-smooth domains*, *Mathematical Methods in the Applied Sciences*, 21 (1998), pp. 823–864.
- [2] P. F. ANTONIETTI, L. MASCOTTO, AND M. VERANI, *A multigrid algorithm for the p -version of the virtual element method*, *ESAIM: Mathematical Modelling and Numerical Analysis*, 52 (2018), pp. 337–364.
- [3] D. N. ARNOLD, *Finite Element Exterior Calculus*, CBMS-NSF Regional Conference Series in Applied Mathematics, Society for Industrial and Applied Mathematics, Dec. 2018.
- [4] L. BEIRÃO DA VEIGA, F. BREZZI, A. CANGIANI, G. MANZINI, L. D. MARINI, AND A. RUSSO, *Basic principles of virtual element methods*, *Mathematical Models and Methods in Applied Sciences*, 23 (2013), pp. 199–214.
- [5] L. BEIRÃO DA VEIGA, F. BREZZI, L. D. MARINI, AND A. RUSSO, *The hitchhiker's guide to the virtual element method*, *Mathematical models and methods in applied sciences*, 24 (2014), pp. 1541–1573.
- [6] S. BERTOLUZZA, M. PENNACCHIO, AND D. PRADA, *Bddc and feti-dp for the virtual element method*, *Calcolo*, 54 (2017), pp. 1565–1593.
- [7] W. BOON AND E. NILSSON, *VirtuE-library*. <https://github.com/WiAErDS/VirtuE>, 2024.
- [8] S. C. BRENNER, Q. GUAN, AND L.-Y. SUNG, *Some estimates for virtual element methods*, *Computational Methods in Applied Mathematics*, 17 (2017), pp. 553–574.
- [9] F. BREZZI, R. S. FALK, AND L. D. MARINI, *Basic principles of mixed virtual element methods*, *ESAIM: Mathematical Modelling and Numerical Analysis*, 48 (2014), pp. 1227–1240.
- [10] A. BUDISA, W. M. BOON, AND X. HU, *Mixed-dimensional auxiliary space preconditioners*, *SIAM Journal on Scientific Computing*, 42 (2020), pp. A3367–A3396.
- [11] J. G. CALVO, *On the approximation of a virtual coarse space for domain decomposition methods in two dimensions*, *Mathematical Models and Methods in Applied Sciences*, 28 (2018), pp. 1267–1289.
- [12] A. CANGIANI, E. H. GEORGIOULIS, T. PRYER, AND O. J. SUTTON, *A posteriori error estimates for the virtual element method*, *Numerische Mathematik*, 137 (2017), pp. 857–893.
- [13] L. CHEN AND J. HUANG, *Some error analysis on virtual element methods*, *Calcolo*, 55 (2018), pp. 1–23.
- [14] L. DA VEIGA, L. MASCOTTO, *Interpolation and stability properties of low-order face and edge virtual element spaces*, *IMA Journal of Numerical Analysis*, 43 (2022), pp. 828–851.
- [15] L. B. DA VEIGA, F. BREZZI, F. DASSI, L. MARINI, AND A. RUSSO, *Lowest order virtual element approximation of magnetostatic problems*, *Computer Methods in Applied Mechanics and Engineering*, 332 (2018), pp. 343–362.
- [16] L. B. DA VEIGA, F. BREZZI, L. D. MARINI, AND A. RUSSO, *$H(\operatorname{div})$ and $H(\operatorname{curl})$ -conforming virtual element methods*, *Numerische Mathematik*, 133 (2016), pp. 303–332.
- [17] L. B. DA VEIGA, F. BREZZI, L. D. MARINI, AND A. RUSSO, *Mixed virtual element methods for general second order elliptic problems on polygonal meshes*, *ESAIM: Mathematical Modelling and Numerical Analysis*, 50 (2016), pp. 727–747.
- [18] L. B. DA VEIGA, F. DASSI, G. MANZINI, AND L. MASCOTTO, *Virtual elements for Maxwell's equations*, *Computers & Mathematics with Applications*, 116 (2022), pp. 82–99.
- [19] F. DASSI AND S. SCACCHI, *Parallel solvers for virtual element discretizations of elliptic equations in mixed form*, *Computers & Mathematics with Applications*, 79 (2020), pp. 1972–1989.
- [20] M. DAUGE, *Elliptic boundary value problems on corner domains: smoothness and asymptotics of solutions*, vol. 1341, Springer, 2006.
- [21] M. DAUGE, *Regularity and singularities in polyhedral domains*, *IRMAR*, (2008), p. 50.
- [22] R. HIPTMAIR AND J. XU, *Nodal auxiliary space preconditioning in $H(\operatorname{curl})$ and $H(\operatorname{div})$ spaces*, *SIAM Journal on Numerical Analysis*, 45 (2007), pp. 2483–2509.
- [23] J. HUANG AND Y. YU, *Some estimates for virtual element methods in three dimensions*, *Computational Methods in Applied Mathematics*, 23 (2023), pp. 177–187.
- [24] K.-A. MARDAL AND R. WINTHER, *Preconditioning discretizations of systems of partial differential equations*, *Numerical Linear Algebra with Applications*, 18 (2011), pp. 1–40.
- [25] L. MASCOTTO, *The role of stabilization in the virtual element method: a survey*, arXiv preprint arXiv:2304.10968, (2023).
- [26] J.-C. NÉDÉLEC, *Mixed finite elements in \mathbb{R}^3* , *Numerische Mathematik*, 35 (1980), pp. 315–341.
- [27] P.-A. RAVIART AND J.-M. THOMAS, *A mixed finite element method for 2-nd order elliptic problems*, *Mathematical aspects of finite element methods*, (1977), pp. 292–315.
- [28] J. XU, *The auxiliary space method and optimal multigrid preconditioning techniques for unstructured grids*, *Computing*, 56 (1996), pp. 215–235.
- [29] Y. ZHU, *Auxiliary space preconditioners for linear virtual element method*, in *Domain Decomposition Methods in Science and Engineering XXV 25*, Springer, 2020, pp. 383–390.